Stem Cell Reports, Volume *15*

Supplemental Information

Electrophysiological Maturation of Cerebral Organoids Correlates with Dynamic Morphological and Cellular Development

Summer R. Fair, Dominic Julian, Annalisa M. Hartlaub, Sai Teja Pusuluri, Girik Malik, Taryn L. Summerfied, Guomao Zhao, Arelis B. Hester, William E. Ackerman IV, Ethan W. Hollingsworth, Mehboob Ali, Craig A. McElroy, Irina A. Buhimschi, Jaime Imitola, Nathalie L. Maitre, Tracy A. Bedrosian, and Mark E. Hester

Figure S1

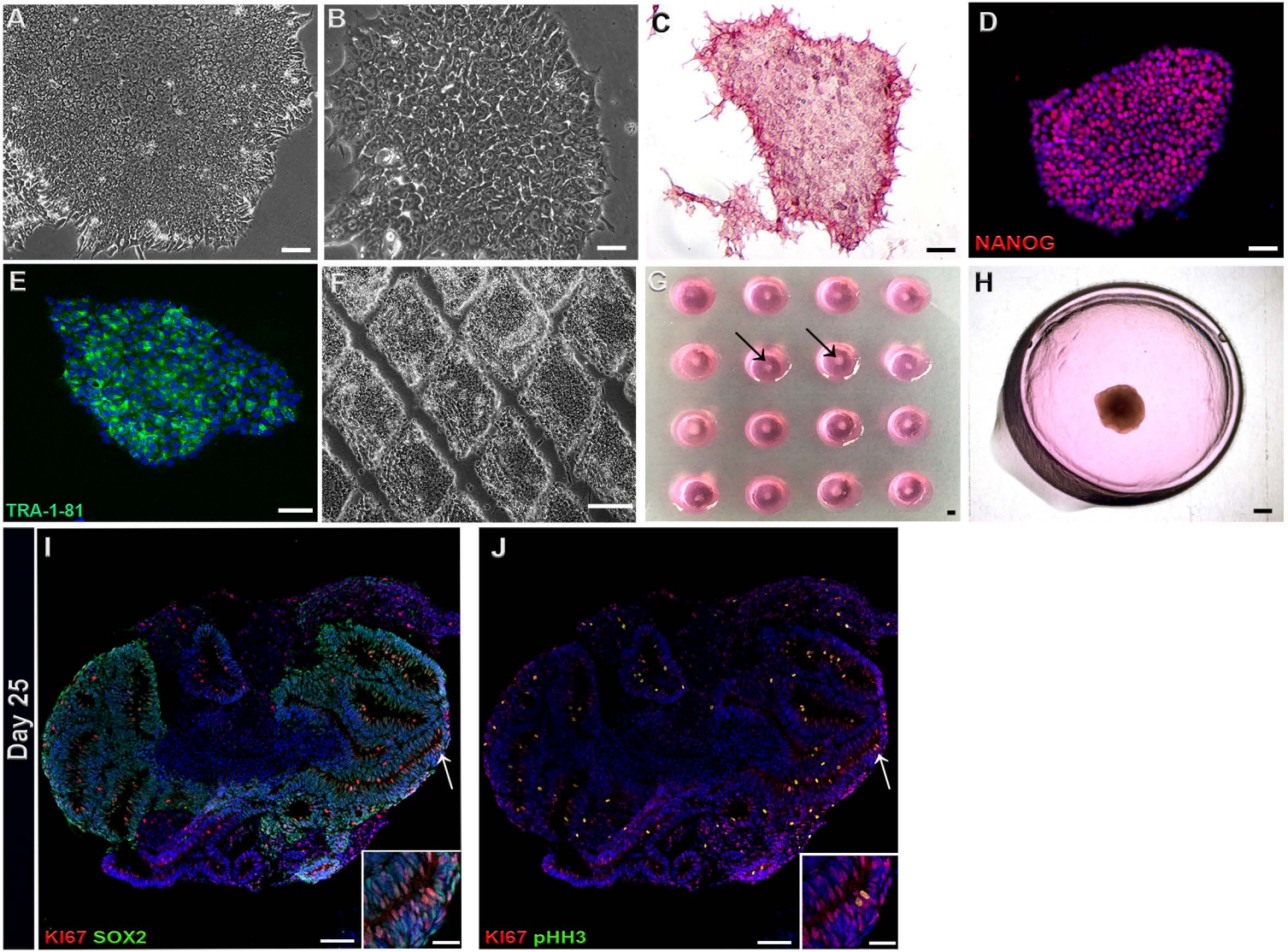

Figure S2

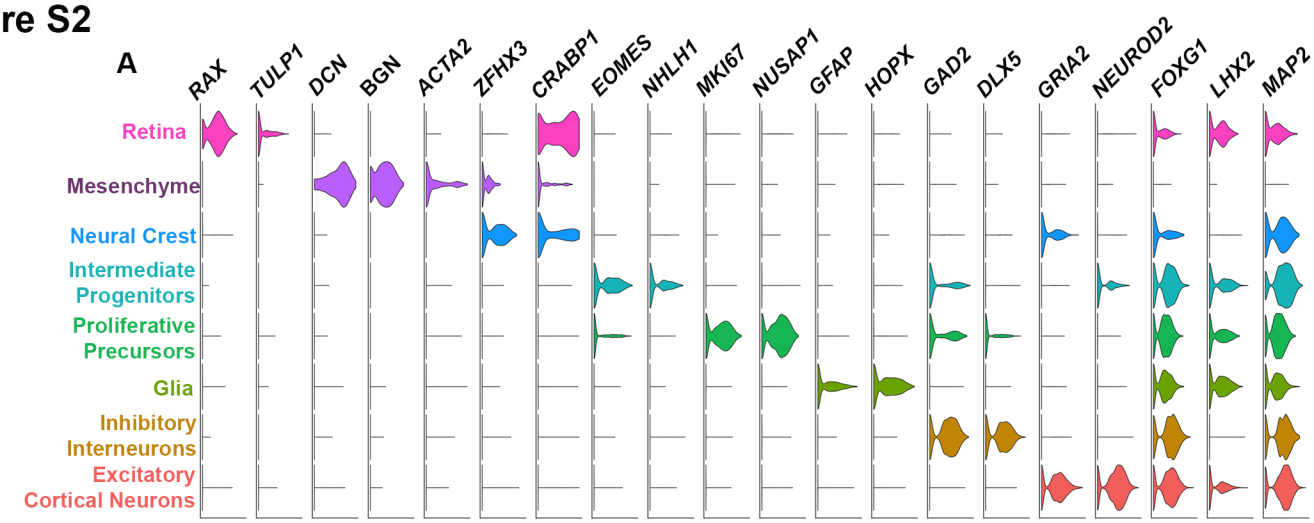
A
RAX
TULP1
DCN
BGN
ACTA2
ZFHX3
CRABP1
EOMES
NHLH1
MKI67
NUSAP1
GFAP
HOPX
GAD2
DLX5
GRIA2
NEUROD2
FOXG1
LHX2
MAP2
Retina
Mesenchyme
Neural Crest
Intermediate Progenitors
Proliferative Precursors
Glia
Inhibitory Interneurons
Excitatory Cortical Neurons

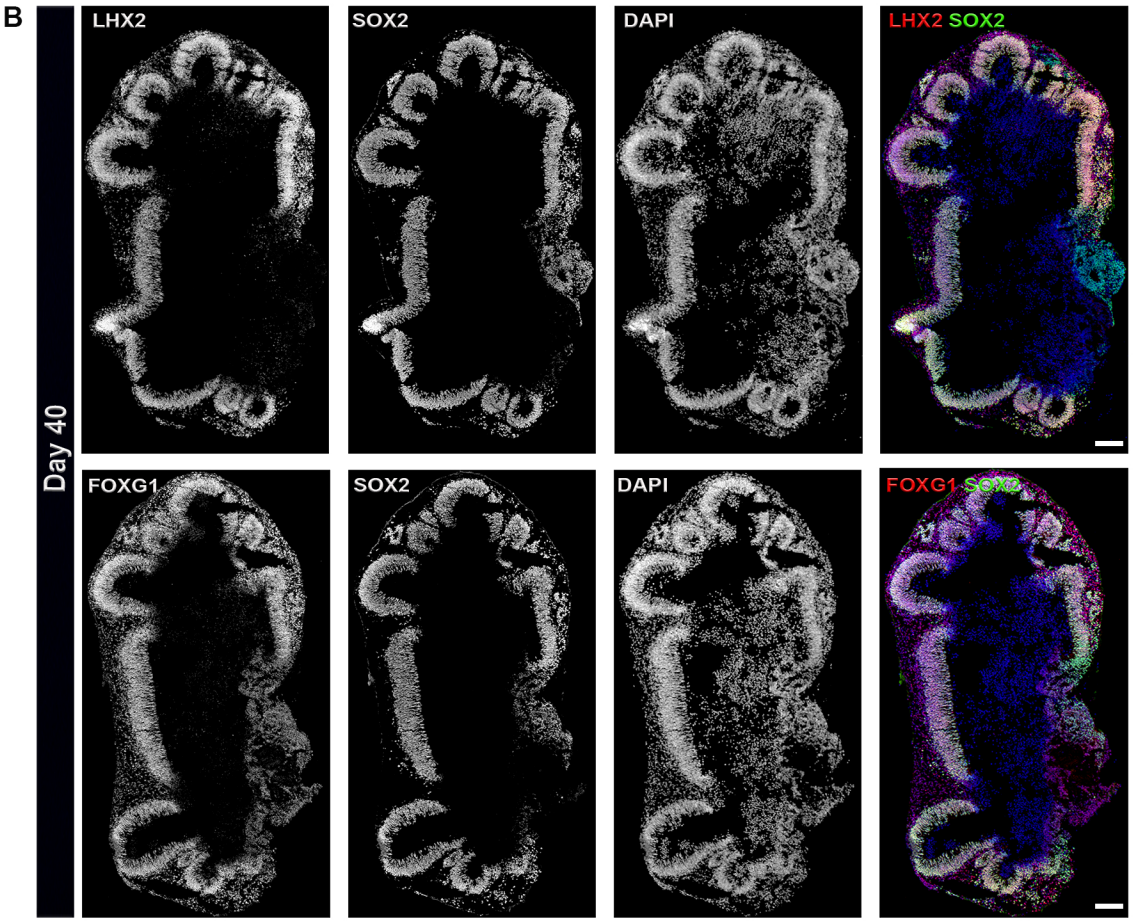
B
Day 40
LHX2
SOX2
DAPI
LHX2 SOX2
FOXG1
SOX2
DAPI
FOXG1 SOX2

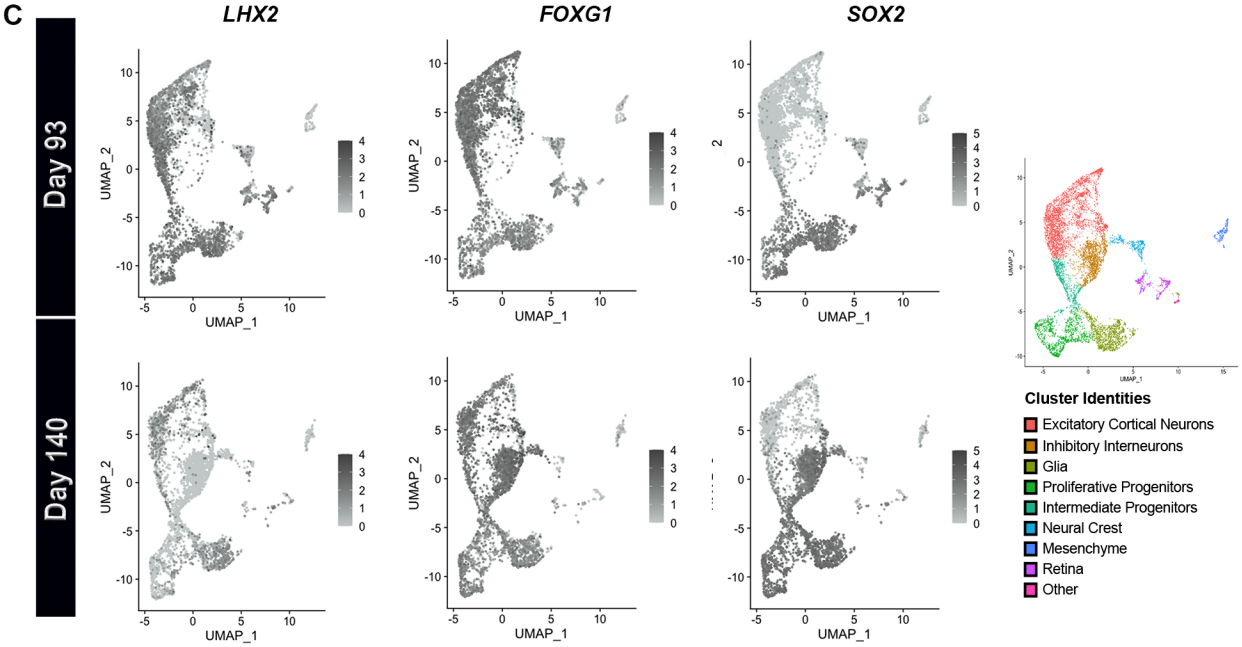
C
LHX2
FOXG1
SOX2
Day 93
Day 140
UMAP_1
UMAP_2
Cluster Identities
Excitatory Cortical Neurons
Inhibitory Interneurons
Glia
Proliferative Progenitors
Intermediate Progenitors
Neural Crest
Mesenchyme
Retina
Other

Figure S3

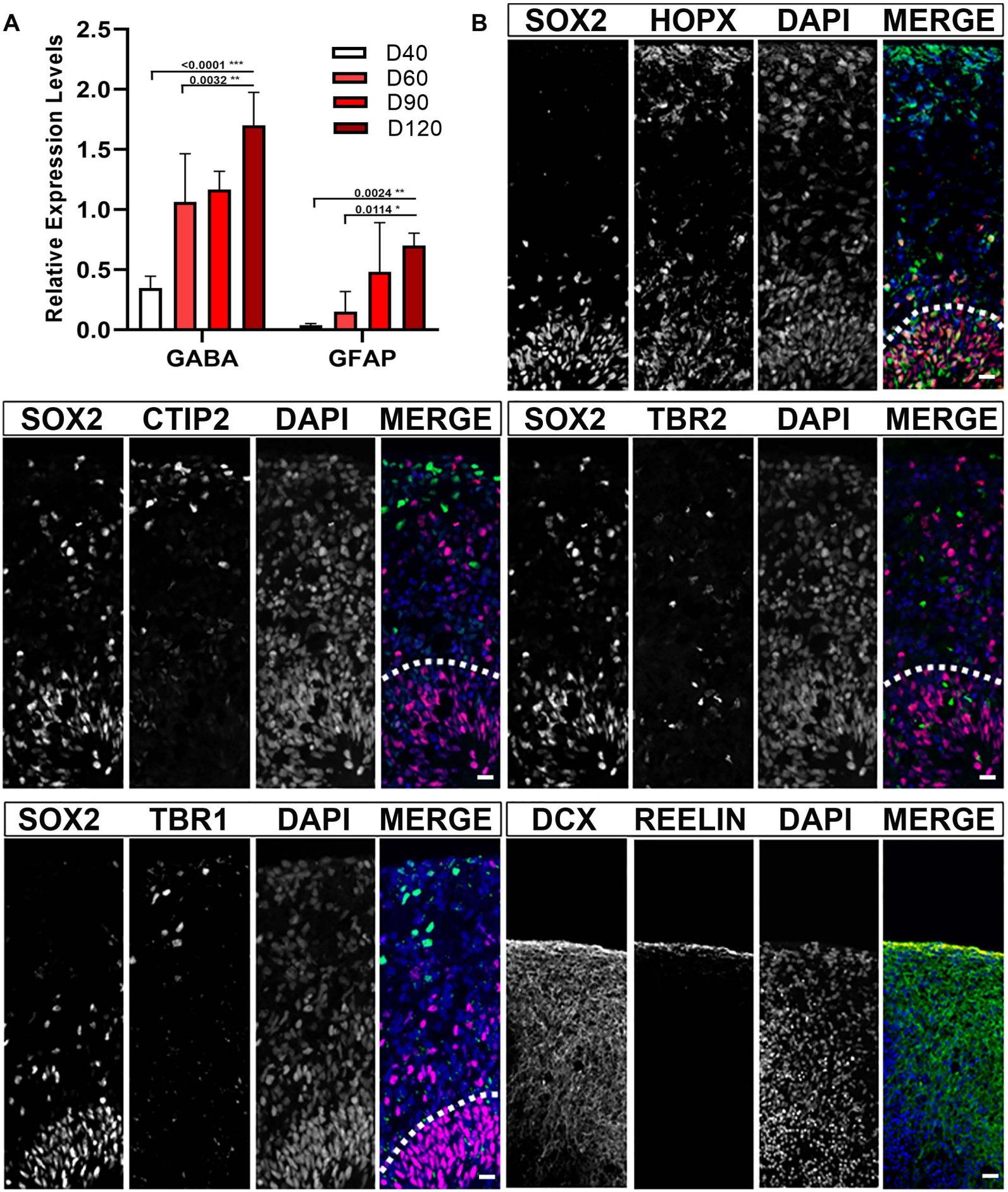
A
Relative Expression Levels
2.5
2.0
1.5
1.0
0.5
0.0
<0.0001 ***
0.0032 **
0.0024 **
0.0114 *
D40
D60
D90
D120
GABA
GFAP
B
SOX2
HOPX
DAPI
MERGE
SOX2
CTIP2
DAPI
MERGE
SOX2
TBR2
DAPI
MERGE
SOX2
TBR1
DAPI
MERGE
DCX
REELIN
DAPI
MERGE

Figure S4

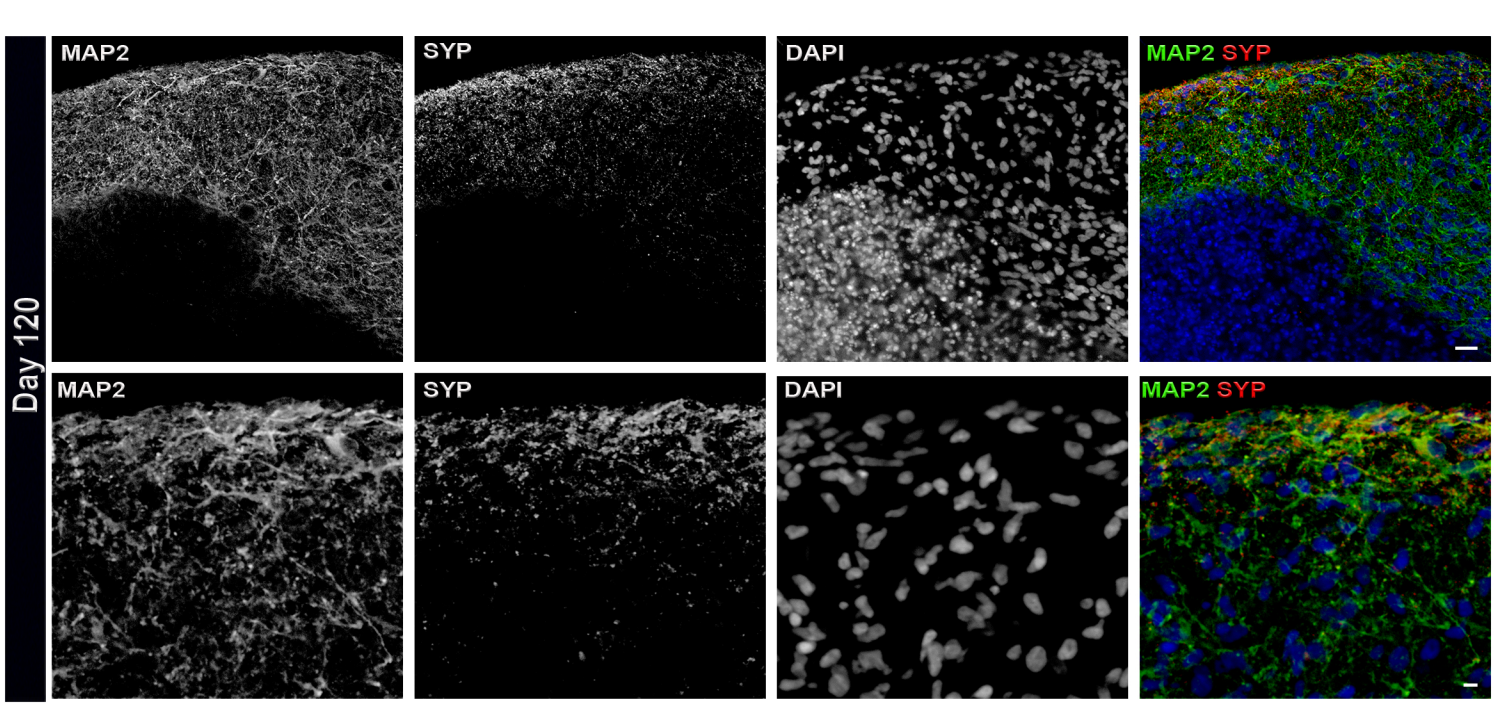
A
Day 120
MAP2
SYP
DAPI
MAP2 SYP
MAP2
SYP
DAPI
MAP2 SYP

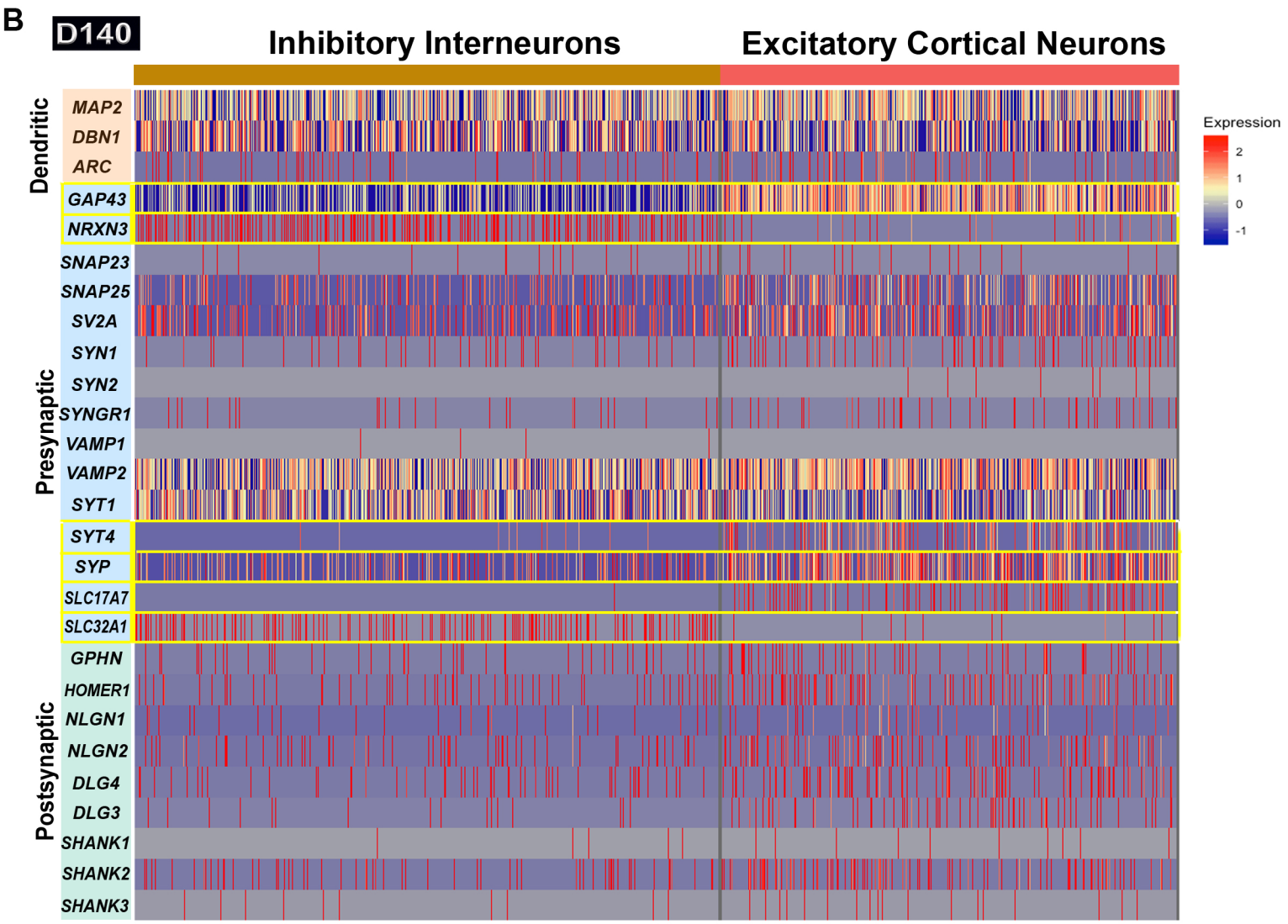
B
D140
Inhibitory Interneurons
Excitatory Cortical Neurons
Dendritic
MAP2
DBN1
ARC
GAP43
NRXN3
Presynaptic
SNAP23
SNAP25
SV2A
SYN1
SYN2
SYNGR1
VAMP1
VAMP2
SYT1
SYT4
SYP
SLC17A7
SLC32A1
Postsynaptic
GPHN
HOMER1
NLGN1
NLGN2
DLG4
DLG3
SHANK1
SHANK2
SHANK3
Expression
2
1
0
-1

Figure S5

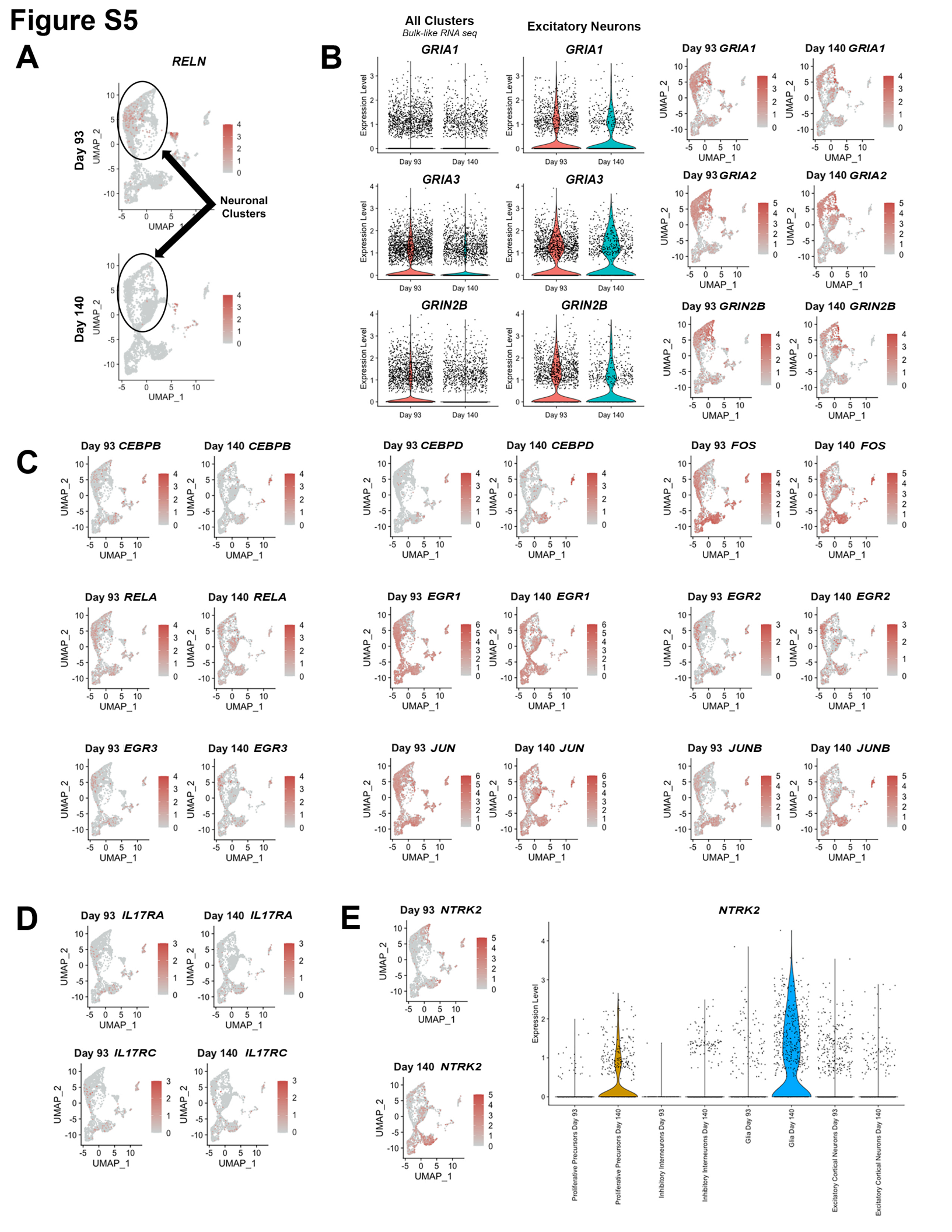
A
RELN
Day 93
Day 140
Neuronal Clusters
UMAP_1
UMAP_2
B
All Clusters
Bulk-like RNA seq
Excitatory Neurons
GRIA1
GRIA3
GRIN2B
Expression Level
Day 93
Day 140
Day 93 GRIA1
Day 140 GRIA1
Day 93 GRIA2
Day 140 GRIA2
Day 93 GRIN2B
Day 140 GRIN2B
C
Day 93 CEBPB
Day 140 CEBPB
Day 93 CEBPD
Day 140 CEBPD
Day 93 FOS
Day 140 FOS
Day 93 RELA
Day 140 RELA
Day 93 EGR1
Day 140 EGR1
Day 93 EGR2
Day 140 EGR2
Day 93 EGR3
Day 140 EGR3
Day 93 JUN
Day 140 JUN
Day 93 JUNB
Day 140 JUNB
D
Day 93 IL17RA
Day 140 IL17RA
Day 93 IL17RC
Day 140 IL17RC
E
Day 93 NTRK2
Day 140 NTRK2
NTRK2
Expression Level
Proliferative Precursors Day 93
Proliferative Precursors Day 140
Inhibitory Interneurons Day 93
Inhibitory Interneurons Day 140
Glia Day 93
Glia Day 140
Excitatory Cortical Neurons Day 93
Excitatory Cortical Neurons Day 140

Figure S6

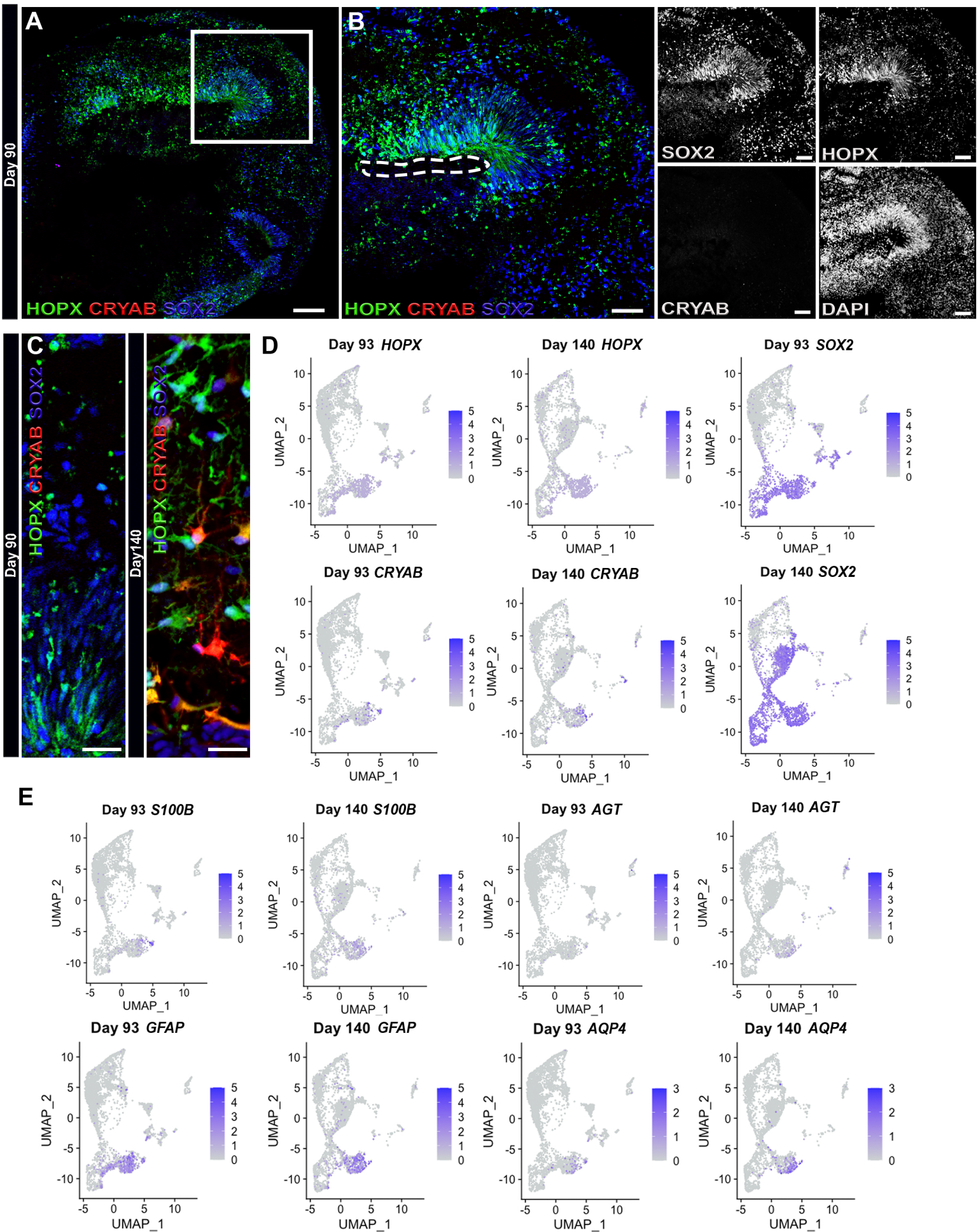
A
B
Day 90
HOPX CRYAB SOX2
HOPX CRYAB SOX2
SOX2
HOPX
CRYAB
DAPI
C
Day 90
Day140
HOPX CRYAB SOX2
HOPX CRYAB SOX2
D
Day 93 HOPX
Day 140 HOPX
Day 93 SOX2
Day 93 CRYAB
Day 140 CRYAB
Day 140 SOX2
E
Day 93 S100B
Day 140 S100B
Day 93 AGT
Day 140 AGT
Day 93 GFAP
Day 140 GFAP
Day 93 AQP4
Day 140 AQP4
UMAP_1
UMAP_2

SUPPLEMENTAL FIGURE LEGENDS

Figure S1. hiPSCs Show Morphological and Molecular Features of Pluripotency and Can Develop into COs that Show Rapid NE Expansion in Early-Stages

(A-B) Phase contrast images of a hiPSC colony showing epithelial morphology and dense growth characteristics. **(C)** Image of a hiPSC colony assayed for alkaline phosphatase activity as indicted by a purple stain. **(D-E)** Immunostaining for pluripotency markers NANOG and TRA-1-81 show robust expression in hiPSCs. DAPI is shown in blue and stains all nuclei. **(F)** Phase contrast image of uniform hiPSC clusters prepared using the StemPro® EZPassage™ tool prior to embryoid body formation. **(G)** NE bodies encapsulated within the center of matrigel droplets as indicated by arrows. **(H)** Higher-magnification image of an enscapsulated NE body. **(I-J)** Immunostains of D25 COs showing rapid expansion and proliferation of SOX2+ NPCs as depicted by the proliferation marker Ki-67 and the mitosis-specific marker phospho-histone H3 (pHH3). DAPI stains nuclei in blue (n=4 organoids). SBs, panel A, 50 μm; panels (B-F, H), 100 μm; panel G, 300 μm; panels (I-J), 100μm, higher magnification inserts, 30μm.

Figure S2. Identification of Cell Clusters in COs Using Specific Gene Markers and Expansion of Neuroepithelium in D40 COs

(A) Violin plots of previously described canonical markers for all clusters. Marker genes are shown along the top horizontal axis and cell clusters are visualized along the vertical axis. **(B)** D40 COs show widespread expression of the telencephalic markers LHX2 and FOXG1 within expanding NE folds, which is co-stained with the proliferative NE marker, SOX2 (n=4 organoids). SBs, panel B, 200 μm. **(C)** Feature UMAP plots from single cell RNA sequencing data for *LHX2, FOXG1*, and *SOX2* expression in D93 and D140 COs.

Figure S3. Dynamic Gene Expression Changes and Diversity of Cortical Neuron Subtypes and Columnar Organizations

(A) Relative gene expression levels of *GABA* and *GFAP* throughout CO development, as determined by RT-PCR. **(B)** D60 COs showing representative images of immunostaining for the NPC marker SOX2 in VZ-like regions, the basal radial glial marker HOPX, and the intermediate progenitor cell marker EOMES, the cortical neuronal pre-plate marker TBR1, the cortical layer 1 marker REELIN, the neuronal migratory marker DCX and the deep layer cortical marker CTIP2. DAPI stains all nuclei and is shown in the merged image of each panel (n=4 organoids). SB in all merged images is 25 μm except for DCX and REELIN panel images where the SB is 50 μm.

Figure S4. Expression of Synaptic Gene Markers in D120 and D140 COs.

(A) IHC stains of D120 COs show MAP2+ neurons that is co-stained with the pre-synaptic marker, SYP, within COs. SB in top-panel images is 25 μm and lower panel images is 10 μm (n=4 organoids). **(B)** Heat map depicting single cell gene expression data of dendritic, presynaptic, and postsynaptic from inhibitory and excitatory neurons in D140 COs.

Figure S5. Single Cell Gene Expression Profiling in D93 and D140 COs.

(A) UMAP plots of *RELN* expression at D93 and D140. Neuronal clusters are encircled to highlight the decrease in *RELN*+ Cajal-Retzius cells by D140. **(B)** AMPA (*GRIA1*, *GRIA3*) and NMDA (*GRIN2B*) receptor expression in COs. Left to right, transcriptomic data are represented as: violin plots of total expression (i.e. bulk RNAseq-like) in all clusters, violin plots of total expression in excitatory neuron cluster only, UMAP plots of expression in all cell types at D93, and UMAP plots of expression in all cell types at D93. **(C)** UMAP plots of all IEGs mentioned in Figure 5 at D93 and D140. **(D)** UMAP plots of *IL-17RA* and *IL-17RC* at D93 and D140. (E) Left, UMAP plots of *NTRK2* at D93 and D140. Right, violin plots depicting *NTRK2* expression in all cell clusters at D93 and D140 (one independent experiment).

Figure S6. Radial Glial Marker Analysis and Single Cell Gene Expression Profiling in D93 and D140 COs.

(A) Low power composite image of HOPX, CRYAB, and SOX2 expression in D90 COs. White frame indicates reference for panel B. **(B)** High power merged and single channel images from inset in panel A. **(C)** Representative panels of radial glia organization around ventricular-like structures in D90 (left) and D140 (right) COs (n=4 organoids). **(D)** Expression of radial glia markers *CRYAB*, *HOPX*, and *SOX2* in all cell clusters at D93 and D140. **(E)** Expression of astrocyte markers *S100B*, *AGT*, *GFAP*, and *AQP4* in all cell clusters at D93 and D140. SB, panel A, 100 μm. All SBs in panel B, 50 μm. SBs, panel C, 20 μm.

Table S1. List of primary antibodies and corresponding information used for immunofluorescence studies.

Table S2. Top Canonical Pathways Enriched in D150 COs. Top-ranked canonical pathways enriched in D150 COs, as indicated by Ingenuity Pathway Analysis (IPA) software. Significance is determined by IPA's default threshold [–log (p-value)>1.3]. The number of genes associated with each canonical pathway is shown from a total of 33 differentially upregulated genes. **Denotes the pathway is associated with NTR/TRK signaling.

Table S3. Comprehensive statistical analyses of EP data as shown in Figure 3. Refer to associated excel file.

Table S4. Statistical summary data from scRNA sequencing analyses as shown in Figure S8.

Table S5. Burst detection parameters used in Mobius Offline Software.

TABLES

Table S1. List of primary antibodies and corresponding information used for immunofluorescence studies.

Antibody	Full Name	Description	Vendor	Catalog #	Species	Dilution
CRYAB	Alpha B Crystallin	Truncated radial glial (tRG) marker	Abcam	ab13496	Ms	1:300
CTIP2	COUP-TF-interacting protein 2	Deep cortical layer 5 marker	Abcam	ab18465	Rat	1:500
DCX	Doublecortin	Microtubule-associated protein associated with neuronal migration	Santa Cruz	sc-8066	Gt	1:200
FOXG1	Forkhead Box G1	Dorsal forebrain marker	Abcam	ab18259	Rb	1:1000
GABA	γ-aminobutyric acid	Major inhibitory neurotransmitter in the CNS	Sigma	A2052	Rb	1:500
GFAP	Glial fibrillary acidic protein	Astrocyte marker	DAKO	Z033429-2	Rb	1:300
HOPX	HOP Homeobox	Outer radial glia marker	Santa Cruz	sc-30216	Rb	1:1000
KI67	Proliferation Marker Protein Ki-67	Marker of all active phases of the cell cycle (G1, SG2, M)	Abcam	ab15580	Rb	1:200
LHX2	LIM Homeobox 2	Dorsal forebrain marker	Abcam	ab184337	Rb	1:200
MAP2	Microtubule Associated Protein 2	Mature neuronal, dendritic marker	Millipore	AB5622	Rb	1:300
NANOG	Homeobox Transcription Factor Nanog	Pluripotency marker	R&D Sys.	AF1997	Gt	1:200
NEUN	Neuronal nuclei	Nuclear localized, mature neuronal marker	Millipore	MAB377	Ms	1:500
PAX6	Paired Box Homeotic Gene-6	Ventricular radial glial marker/forebrain marker	Biolegend	901301	Rb	1:300
pHH3	Phospho-Histone H3	M-phase specific proliferation marker	Millipore	06-570	Rb	1:500
PVA	Parvalbumin	Ca2+-binding, cortical GABAergic interneuron marker	Swant	PV27	Rb	1:300
P-VIMENTIN	Phosphorylated Vimentin	Dividing radial glial (RG) marker	MBL	D076-3S	Ms	1:1000
RELN	Reelin	Marginal zone/cortical layer 1 marker	Millipore	MAB5366	Ms	1:300
S100 Beta	S-100 calcium-binding protein, beta chain	Glial specific marker expressed by a subtype of mature astrocytes.	Sigma	s26-44	Rb	1:300
SATB2	Special AT-rich sequence-binding protein 2	Superficial, late-born cortical layer II-IV marker	Abcam	ab51502	Ms	1:300
SMI32	clone SMI-32, non-phosphorylated neurofilament H	Neural axonal marker	Millipore	NE1023	Ms	1:1000
SOX2	SRY-Box 2	Neural progenitor cell marker	Santa Cruz	sc-17320	Gt	1:200
SST	Somatostatin	Neuropeptide that is specific to a class of cortical GABAergic interneuron subtype	Santa Cruz	sc-74556	Rb	1:300
SYP	Synaptophysin	Pre-synaptic neural marker	Millipore	MAB329	Ms	1:1000
TBR1	T-Box, Brain 1	Early born, pre-plate cortical marker	Abcam	Ab31940	Rb	1:500
TBR2	T-Box, Brain 2	Intermediate progenitor (IP) marker	Abcam	Ab23345	Rb	1:300
TRA-1-81	Podocalyxin	Surface protein expressed on human pluripotent stem cells	Thermo-Fisher	41-1100	Ms	1:200
TUJ1	Neuron-specific Class III β-tubulin	Immature neural marker	Biolegend	801201	Ms	1:500
VGLUT1	Vesicular glutamate transporter 1(SLC17A7)	Glutamatergic (excitatory) neural marker	Millipore	MAB5502	Ms	1:300

Table S2. Top Canonical Pathways Enriched in D150 COs. Top canonical pathways enriched in D150 COs and associated [–log (p-value). Significance is determined by IPA's default threshold [–log (p-value)>1.3]. The number of genes associated with each canonical pathway is shown from a total of 33 differentially upregulated genes. **Denotes the pathway is associated with NTR/TRK signaling.

Canonical Pathways	-log(p-value)	Associated Number of Genes (from a total of 33)
1.) IL-17A Signaling in Fibroblasts	13.2	7
2.) **Neuropathic Pain Signaling In Dorsal Horn Neurons	13.1	9
3.) Synaptic Long Term Potentiation	10.9	8
4.) IL-17A Signaling in Gastric Cells	9.53	5
5.) Neuroinflammation Signaling Pathway	9.21	9
6.) Role of Macrophages, Fibroblasts and Endothelial Cells in Rheumatoid Arthritis	9.09	9
7.) PI3K Signaling in B Lymphocytes	8.94	7
8.) Neurotrophin/TRK Signaling	8.59	6
9.) Estrogen-Dependent Breast Cancer Signaling	8.5	6
10.) Regulation of IL-2 Expression in Activated and Anergic T Lymphocytes	8.5	6

Table S3. Comprehensive statistical analyses of EP data as shown in Figure 3. Please see associated excel file.

Table S4. Statistical summary data from scRNA sequencing analyses as shown in Figure S8.

Gene	p_val	avg_diff	pct.1 (d93)	pct.2 (d140)	p_val_adj
CEBPD	5.67E-39	-0.2878	0.031	0.1	1.17E-34
NTRK2	1.33E-37	-0.37999	0.11	0.207	2.73E-33
JUNB	1.06E-25	-0.73513	0.18	0.266	2.18E-21
JUN	8.47E-17	0.008603	0.612	0.509	1.74E-12
EGR1	1.26E-11	0.258736	0.579	0.527	2.59E-07
EGR2	1.91E-10	-0.07197	0.077	0.116	3.93E-06
CEBPB	0.000381	-0.01504	0.059	0.042	1
IL17RA	0.023139	-0.01094	0.026	0.035	1
EGR3	0.028882	-0.02342	0.051	0.061	1
IL17RC	0.139015	0.00363	0.024	0.02	1
RELA	0.287542	-0.00825	0.122	0.13	1
FOS	0.296907	-0.33782	0.441	0.456	1

Table S5. Burst detection parameters utilized in Mobius Offline Software.

Burst Detection Parameters	
maximum interval to start burst	300ms
maximum interval to end burst	301ms
minimum number of spikes in a burst*	10 spikes
minimum duration of a burst	50 ms
minimum interval between bursts	200ms
*except for the D34 time point containing 5 minimum number of spikes	
Network Burst Detection Parameters	
minimum percentage of active electrodes	25%
minimum threshold	1,100 spikes/second
bin size	100ms

SUPPLEMENTAL EXPERIMENTAL PROCEDURES

Immunofluorescence analysis. COs, from various designated developmental time points (n=4 from each developmental stage), were transferred to a 4% paraformaldehyde (PFA) solution in PBS and allowed to fix overnight at 4°C. COs were then transferred to a 10% sucrose/PBS solution and allowed to sink before transferring to a 30% sucrose/PBS solution. After COs sank within the 30% sucrose/PBS solution, they were transferred to an embedding tray and immersed in O.C.T (Sakura, Tokyo, Japan). Without introducing air bubbles, COs were then gently moved within the center of the O.C.T solution with a pipette tip. Embedded COs were then rapidly frozen in a dry ice/methanol bath, transferred to a cryostat chuck, and sectioned at 20μm slices using a cryostat (ThermoFisher). Sections were placed onto positively charged glass slides and stored at -20 °C until further immunofluorescence analysis. To perform immunofluorescence analysis, sections were re-hydrated with Tris-buffered saline (TBS), and then incubated in blocking solution containing 0.1% triton X-100 and 10% donkey serum in TBS for 1 hour at RT. Organoid sections were then incubated with primary antibodies at the concentrations designated in Table S1 for 24 hours at 4°C. Sections were then washed with TBS three times for five minutes each before incubation with the secondary Alexa Fluor conjugated antibodies (ThermoFisher) at a 1:500 dilution in blocking solution for two hours at RT. After this incubation, sections were washed with TBS three times for five minutes each and cover-slipped with ProLong Gold Antifade Mountant with DAPI. Primary antibodies and their corresponding descriptions used in this study are shown in Table S1. Confocal microscopy acquisition was performed with a Zeiss LSM confocal fluorescence microscope (models 700 and 800). Fluorescence intensity of GABA and GFAP labeling was performed by acquiring low power images of whole organoid sections from 4 separate COs and then were analyzed using ImageJ software.

Gene expression and pathway analysis. Profiling for genes involved in synaptic plasticity was performed using the RT2 Profile PCR Array human synaptic plasticity kit (Qiagen, Cat # PAHS-126A-2) and the RT2 SYBR Green/ROX PCR Master mix (Qiagen, Cat # 330522) using an ABI Step One plus Real time PCR machine. This gene array

includes primers for 84 transcripts involved in synaptic plasticity, thus allowing for identification of novel gene expression pathways. In brief, total RNA was extracted and purified from the iPS-1 cell line, neuroectodermal bodies, and from the pooling of 5 COs from designated time points using the RNeasy Plus Mini Kit (Qiagen). Three independent qRT-PCR experiments were performed from all samples in this analysis. Data analyses were performed using the GeneGlobe Data Analysis Center Software available on the Qiagen website (https://www.qiagen.com/us/shop/genes-and-pathways/data-analysis-center-overview-page/). Normalization of gene expression was performed using a set of five housekeeping genes and fold regulation was calculated relative to the control iPS-1 cell line. The web tool called Clustvis was used to cluster the row of genes using the Euclidean average clustering method (Metsalu and Vilo, 2015). Fold-change values relative to control hiPSCs were used as input for Clustvis. Genes that were upregulated at three-fold or higher levels within samples relative to control were uploaded into the Ingenuity Pathway Analysis software to identify canonical pathways that involve the upregulated genes, which were then ranked by a statistical scoring algorithm using p-value calculations.

scRNA-seq sample analysis and data processing. Each CO was dissociated into a single cell suspension using a gentleMACS Octo Dissociator (Miltenyi) according to the manufacturer's 37-ABDK02 protocol. In brief, COs were placed in a gentleMACS C Tube (one organoid per C-tube, Miltenyi, 130-093-237) that contained a 2mL solution of Accumax (Sigma, A7089) and then processed on the Octo Dissociator. A 10mL solution of dPBS with 0.04% BSA (Sigma, A9418) was then added to each sample and filtered at 70μm to remove debris. Cell mixtures were then pelleted and resuspended in 1mL dPBS/0.04% BSA. Suspensions were subjected to a second filtration step with a 40μm Flowmi® cell strainer (Sigma, BAH136800040). The concentration and viability of each suspension was determined with a trypan blue stain and hemocytometer.

Raw base call sequencing data were demultiplexed in Illumina’s bcl2fastq and subsequently processed with the 10x Genomics Cell Ranger (v3.1.0) pipeline using data quality that was assessed with the ‘count’ function summary output (D93: 6,172 cells, 23,932 mean reads per cell, 1,762 median genes per cell, 3,988 median UMI counts per

cell; D140: 4,479 cells, 25,435 mean reads per cell, 1,910 median genes per cell, 4,458 median UMI counts per cell) prior to downstream analysis.

Count matrices were loaded into Seurat v3.1.0 (Butler et al., 2018; Stuart et al., 2019) to remove batch effects and apply standard quality control parameters. In brief, cells with <200 and >5,000 unique features or >20% mitochondrial reads were removed from the datasets (4,491 cells from D93 and 4,087 cells from D140 passed). Each organoid's raw UMI count was normalized to its respective total UMI using log-normalization with a scale factor of 10,000 and the top 2,000 variable features per object were identified prior to integration. Integration anchors were identified with 30 principal components and used to combine the two organoid datasets into a single object with a total of 8,578 cells. Then, a linear transformation and dimension reduction analysis (PCA) was applied prior to running a uniform manifold approximate and projection analysis. The dimensionality of this analysis was determined with an elbow plot rank. The FindNeighbors (PCA reduction, 20 dimensions) and FindClusters (0.5 res, 20 dim) Seurat functions were used to carry out KNN unbiased clustering resulting in a total of 13 unbiased clusters. Each cluster's conserved differentially expressed genes were identified with the FindAllMarkers function (Wilcoxon test, min.pct = 0.25, minlogFC = 0.25). These criteria were further refined to only consider a minimum 1.0 log-fold change and two-sided t-test $p<0.05$. The ratio of cells within a given cluster to cells within all other clusters expressing a given marker was also taken into consideration for each defining marker. After evaluating inter- and intra-cluster expression patterns of characteristic canonical markers (Cakir et al., 2019; Quadrato et al., 2017; Velasco et al., 2019) clusters were collapsed into nine categories. Further integrated analyses and visual representations were generated with Seurat and its dependencies.

MEA. Acquisition of spontaneous extracellular field potentials in whole-brain COs was acquired with a 64-channel MEA system (MED64 system, Alpha Med Scientific) at a sampling rate of 20 kHz/channel and at 37°C using a temperature controller device. The MED64 system was connected to a Dell Precision T1700 Tower workstation equipped with an Intel Core i7 4790 (3.6 Ghz) processor. MEA probes (Alpha Med Scientific, Cat # MED-P515A, 64 electrodes, 50μm diameter/100μm spacing) were treated with 0.005%

Polyethyleneimine (PEI) in 25 mM borate buffer (pH 8.4) for ten minutes at RT and then coated with Laminin (Thermofisher, Cat # 23017-015) at a concentration of 2 µg/ml and incubated at 37°C for one hour prior to recording. At D34, we selected 20 COs with similar shape and size that lacked cystic structures to record. We randomly selected 4 of the pre-selected COs at each time point to perform our analyses. To record EP signals, COs (n=4) were transferred from culture to the center of the probe containing the 8x8 channel array using a 1mL pipette with a 1mL tip that was previously cut to a 5mm diameter. Conditioned organoid culture media (approximately ~150 µl) was then placed on the surface of the probe to allow the CO to maintain close proximity with the microelectrodes. Three-minute recordings were performed from all 64 electrode sites, similar to previous studies (Kathuria et al., 2020; Trujillo et al., 2019). Once complete, the COs were placed back into long-term shaking culture conditions. Spikes were detected from raw data using a threshold of 4.25x the SD of the raw signal (Figure 1). Spike data were then imported into MED64 Mobius Offline software (Version 1.4.5) and EP metrics were determined. Electrodes are defined as active by detecting at least 5 spikes/minute (McConnell et al., 2012; Novellino et al., 2011). See Table S5 for burst detection parameters.

REFERENCES

Butler, A., Hoffman, P., Smibert, P., Papalexi, E., and Satija, R. (2018). Integrating single-cell transcriptomic data across different conditions, technologies, and species. Nature biotechnology *36*, 411-420.

Cakir, B., Xiang, Y., Tanaka, Y., Kural, M.H., Parent, M., Kang, Y.J., Chapeton, K., Patterson, B., Yuan, Y., He, C.S.*, et al.* (2019). Engineering of human brain organoids with a functional vascular-like system. Nat Methods *16*, 1169-1175.

Kathuria, A., Lopez-Lengowski, K., Vater, M., McPhie, D., Cohen, B.M., and Karmacharya, R. (2020). Transcriptome analysis and functional characterization of cerebral organoids in bipolar disorder. Genome Med *12*, 34.

McConnell, E.R., McClain, M.A., Ross, J., Lefew, W.R., and Shafer, T.J. (2012). Evaluation of multi-well microelectrode arrays for neurotoxicity screening using a chemical training set. Neurotoxicology *33*, 1048-1057.

Metsalu, T., and Vilo, J. (2015). ClustVis: a web tool for visualizing clustering of multivariate data using Principal Component Analysis and heatmap. Nucleic acids research *43*, W566-570.

Novellino, A., Scelfo, B., Palosaari, T., Price, A., Sobanski, T., Shafer, T.J., Johnstone, A.F., Gross, G.W., Gramowski, A., Schroeder, O.*, et al.* (2011). Development of micro-electrode array based tests for neurotoxicity: assessment of interlaboratory reproducibility with neuroactive chemicals. Frontiers in neuroengineering *4*, 4.

Quadrato, G., Nguyen, T., Macosko, E.Z., Sherwood, J.L., Min Yang, S., Berger, D.R., Maria, N., Scholvin, J., Goldman, M., Kinney, J.P.*, et al.* (2017). Cell diversity and network dynamics in photosensitive human brain organoids. Nature *545*, 48-53.

Stuart, T., Butler, A., Hoffman, P., Hafemeister, C., Papalexi, E., Mauck, W.M., 3rd, Hao, Y., Stoeckius, M., Smibert, P., and Satija, R. (2019). Comprehensive Integration of Single-Cell Data. Cell *177*, 1888-1902.e1821.

Trujillo, C.A., Gao, R., Negraes, P.D., Gu, J., Buchanan, J., Preissl, S., Wang, A., Wu, W., Haddad, G.G., Chaim, I.A.*, et al.* (2019). Complex Oscillatory Waves Emerging from Cortical Organoids Model Early Human Brain Network Development. Cell stem cell *25*, 558-569 e557.

Velasco, S., Kedaigle, A.J., Simmons, S.K., Nash, A., Rocha, M., Quadrato, G., Paulsen, B., Nguyen, L., Adiconis, X., Regev, A.*, et al.* (2019). Individual brain organoids reproducibly form cell diversity of the human cerebral cortex. Nature.